I. Transient Absorption Spectroscopy

Setup

The femtosecond laser setup used to record the transient absorption (TA) data was based on a Spitfire Pro XP amplifier seeded by a Mai Tai (both from Spectra-Physics). The central output wavelength was 795 nm with a 60 fs pulse length delivered at 1 kHz repetition frequency. The beam was split along two pathways; one pumping a collinear optical parametric amplifier (TOPAS-C, Light Conversion) to generate the pump beam. The other was led through a delay line and used to generate the white-light continuum probe using a 3 mm CaF_2 translating optical window. The probe pulse was split into two parts; the first directed towards the sample where it was overlapped with the collinear pump pulse, the other used as reference. The probe and reference beams were brought to the slit of a spectrograph and dispersed onto a double photodiode array, each with 512 elements (Pascher Instruments). The mutual polarization between pump and probe beams was set to 54.7° by placing Berek compensator in the pump beam.

Experimental Conditions

The $[Fe(bpy)_2(CN)_2]$ sample in methanol solution was measured in a 1 mm quartz cuvette and prepared at a concentration resulting in an OD of 0.3 at the 550 nm pump wavelength. To determine the Group Velocity Dispersion (GVD) of the probe light, the cross-phase modulation signal was measured for the neat solvent under identical experimental conditions. The intensity of the pump pulses was kept below 10^{14} photons/cm^2/pulse.

Data Treatment

A correction curve for the GVD was determined from the cross-phase modulation signal and used to correct time-zero for each recorded spectrum. For the spectra used to analyze the sub picosecond dynamics, the cross-phase modulation signal was scaled to, and subtracted from the data before analysis.

Global Analysis

The excited state kinetics were first investigated in a principal component analysis framework based on singular value decomposition of the datasets as described in Liu et al.[1] Multi-exponential fitting to the time-evolution of the singular vectors returned the characteristic timescale of the evolution of the transient data forming the base for the global analysis (GA).

The GA of $[Fe(bpy)_2(CN)_2]$ data returns an instrument response function (IRF) of 85 ± 11 fs (FWHM, shown in Figure S1E), and yields three decay associated spectra (DAS) shown in Figure S1(D). A short-lived (120 ± 37 fs) DAS1 with a clear maximum around 370 nm and a weaker absorption between 400 nm and 550 nm, a weak DAS2 with a 1.5 ± 0.4 ps lifetime, and a DAS3 with a 250 ± 11 ps lifetime with bleach features matching the steady-state absorption features.

Fig. S1. $[Fe(bpy)_2(CN)_2]$ in methanol two-dimensional time-dependent change in UV visible absorption data. (A) Experimental difference spectra and (B) global analysis fit. (C) Residuals and (D) the resulting decay associated spectra. (E) Kinetics at 370 nm and 560 nm with the IRF.

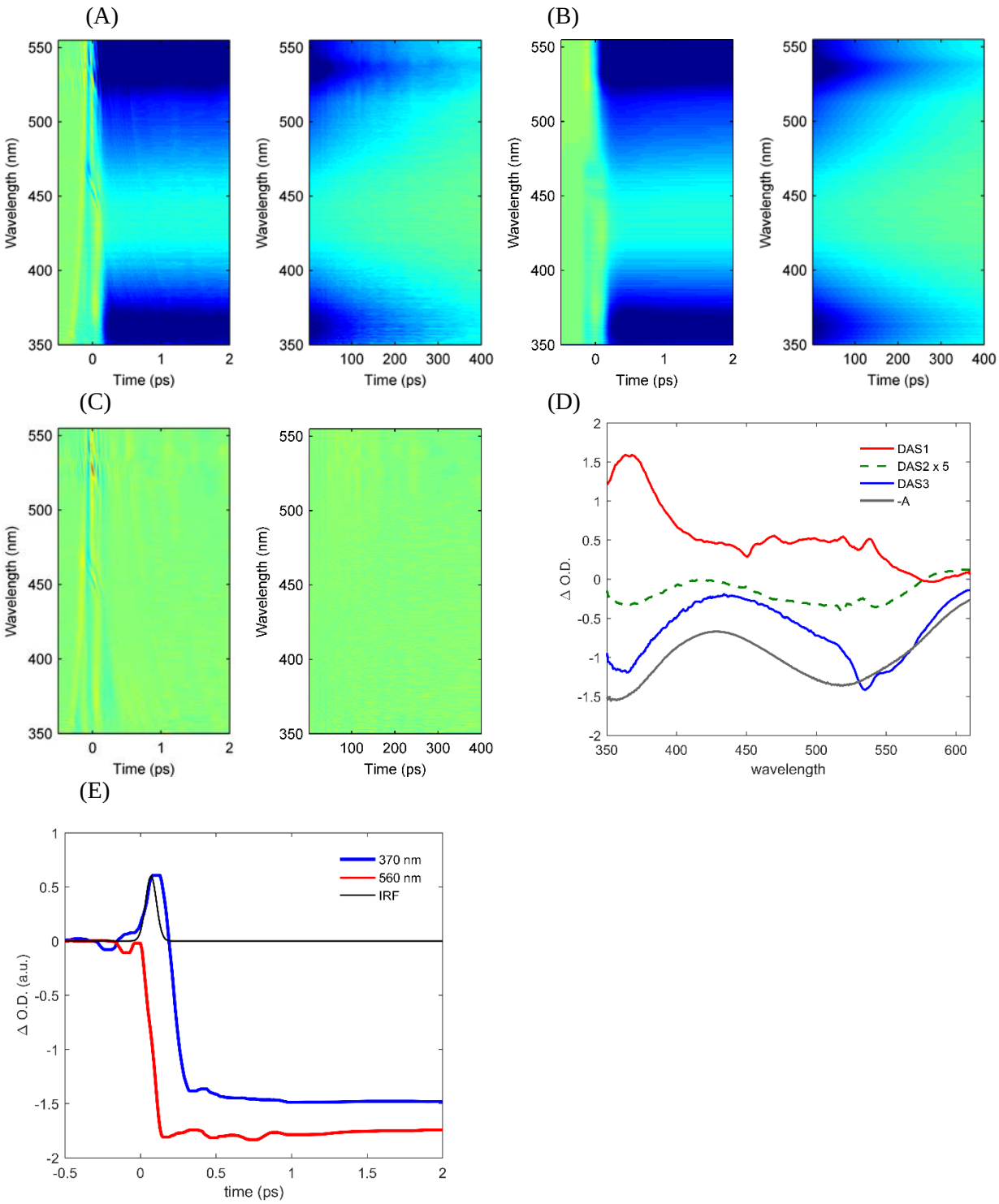

II. X-ray Emission Spectroscopy

Setup

The setup for X-ray Emission Spectroscopy at the X-ray Pump Probe (XPP) beamline at the Linear Coherent Light Source (LCLS) is similar to the one described in the Online Method section of Zhang et. al [2]. The experiment used a 0.1 mm thick planar liquid jet oriented at an angle of 45° with respect to the direction of the incident X-ray beam. The sample solution was collinearly excited with a 70 fs FWHM visible laser beam generated by optical parametric amplification of the 800 nm output of a Ti:sapphire regenerative amplifier laser system (Coherent, Legend). The 8 keV x-ray laser pulses, with an average bandwidth of 0.3%, were focused using Be compound refractive lenses to a 200 μm diameter spot size at the sample position.

The incoming x-ray pulse energy was measured using noninvasive diagnostics before the sample. A high-resolution energy dispersive x-ray emission spectrometer [3], based on the von Hamos geometry, was used to capture the Fe 3p-1s (Kβ) fluorescence. The spectrometer was equipped with 4 cylindrically bent (500 mm radius) Ge(620) crystal analyzers and the central Bragg angle was set to 79.1 degrees. A CSPAD 2D pixel array detector (388x356 pixels) intersected x-rays diffracted from the crystal analyzers in the energy range from 7028-7084 eV [4].

Data Treatment

The CSPAD detector recording the Kβ emission was calibrated through a pixel dependent dark current (pedestal) subtraction, a common mode off-set subtraction, and an experimentally determined gain map. The gain map was built from histograms of each pixel response extracted from multiple images (after dark current and common mode subtraction) collected over many minutes. Gaussians were fit to the zero and one photon peaks of the histograms, enabling fine-tuned dark and gain corrections to the histograms directly from the data. The zero photon peaks were centered at zero analog-to-digital units and the separation between the zero and one photon peaks were scaled to unity for all pixels. The counts for each pixel in a given time-step were obtained by averaging the analog-to-digital values above a threshold of

2.5σ of the zero-photon peak and scaling to the incident x-ray intensity. The final 1D spectrum for each time-step was obtained by integrating the signal in the nondispersive direction as described in [5].

The shot-to-shot x-ray-optical relative time of arrival fluctuations were measured for every x-ray-optical pulse pair with a timing diagnostic tool based on optical detection of x-ray generated carriers in a Si3N4 thin film [6]. This experimental measure of the relative timing was used to sort each experimental shot by the relative time of arrival. Thus, the final time resolution of the experiment results from the convolution of the optical and x-ray pulse durations, the difference group velocity of the x-ray and optical pulses in the sample, and the error in the relative time of arrival measurement. These set the resolution to roughly 150 fs FWHM.

Experimental Conditions

Samples consisted of 25mM $[Fe(bpy)_2(CN)_2]$ in methanol solution, resulting in an OD of 1 at the 550 nm pump wavelength. The intensity of the pump pulses was set to 4×10^{14} photon/cm^2/pulse to match the increased concentration compared to the TA measurements.

III. Modeling of the Transient X-ray Emission Measurements

We have utilized two distinct mechanisms for photo excited MLCT excited state return to the electronic ground state: (1) relaxation of the MLCT excited state to the ground state via a ^{5}MC excited state where the quintet state is formed directly from the MLCT, and (2) relaxation of the MLCT excited state to the ground state via a ^{5}MC excited state where the MLCT decays to a transient ^{3}MC before forming a ^{5}MC.

1. Relaxation of the MLCT excited state to the ground state via a ^{5}MC excited state where the quintet state is formed directly from the MLCT:

$$\mathrm{MLCT} \xrightarrow{k_1} {}^5\mathrm{MC} \xrightarrow{k_3} \mathrm{G}$$

where MLCT corresponds to the electronic excited state populated by optical excitation, ^{5}MC corresponds to the quintet ligand field state, and G represents the electronic ground state. The differential rate equations for each species are given by the following mass balance simultaneous equations,

$$\frac{d[\mathrm{MLCT}]}{dt} = -k_1[\mathrm{MLCT}]$$
$$\frac{d[{}^5\mathrm{MC}]}{dt} = k_1[\mathrm{MLCT}] - k_3[{}^5\mathrm{MC}]$$
$$\frac{d[\mathrm{G}]}{dt} = k_3[{}^5\mathrm{MC}]$$

The integrated rate equations that provide the following time-dependent populations for the three species,

$$[\mathrm{MLCT}] = [\mathrm{MLCT}]_0 e^{-k_1 t}$$
$$[{}^5\mathrm{MC}] = [\mathrm{MLCT}]_0 \frac{k_1}{k_3 - k_1}(e^{-k_1 t} - e^{-k_3 t})$$
$$[\mathrm{G}] = [\mathrm{MLCT}]_0 - [\mathrm{MLCT}] - [{}^5\mathrm{MC}]$$

From the UV-visible measurement, we know the ^{5}MC state has a lifetime of roughly 250 ps. The long lifetime of the ^{5}MC excited state allows us to set $k_3 \cong 0$ when we model the kinetics in the first couple of picoseconds. The integrated rate equations can be reduced to,

$$[\text{MLCT}] = [\text{MLCT}]_0 e^{-k_1 t}$$
$$[^5\text{MC}] = [\text{MLCT}]_0 (1 - e^{-k_1 t})$$

2. Relaxation of the MLCT excited state to the ground state via a ^{5}MC excited state where the MLCT decays to a transient ^{3}MC before forming a ^{5}MC:

$$\text{MLCT} \xrightarrow{k_1} {}^3\text{MC} \xrightarrow{k_2} {}^5\text{MC} \xrightarrow{k_3} \text{G}$$

where MLCT corresponds to the electronic excited state populated by optical excitation, ^{3}MC corresponds to the triplet ligand field excited state, and ^{5} MC corresponds to the quintet ligand field excited state, and G represents the electronic ground state. The differential rate equations for each species are given by the following mass balance simultaneous equations,

$$\frac{d[\text{MLCT}]}{dt} = -k_1[\text{MLCT}]$$
$$\frac{d[^3\text{MC}]}{dt} = k_1[\text{MLCT}] - k_2[^3\text{MC}]$$
$$\frac{d[^5\text{MC}]}{dt} = k_2[^3\text{MC}] - k_3[^5\text{MC}]$$
$$\frac{d[\text{G}]}{dt} = k_3[^5\text{MC}]$$

The integrated rate equations that provide the following time-dependent populations for the four species,

$$[\mathrm{MLCT}] = [\mathrm{MLCT}]_0 e^{-k_1 t}$$

$$[^3\mathrm{MC}] = [\mathrm{MLCT}]_0 \frac{k_1}{k_2 - k_1}(e^{-k_1 t} - e^{-k_2 t})$$

$$[^5\mathrm{MC}] = [\mathrm{MLCT}]_0 \frac{k_1 k_2[(k_3 - k_2)e^{-k_1 t} - (k_3 - k_1)e^{-k_2 t} + (k_2 - k_1)e^{-k_3 t}]}{(k_2 - k_1)(k_3 - k_2)(k_3 - k_1)}$$

$$= [\mathrm{MLCT}]_0 \frac{k_1 k_2[k_3(e^{-k_1 t} - e^{-k_2 t}) + k_2(e^{-k_3 t} - e^{-k_1 t}) + k_1(e^{-k_2 t} - e^{-k_3 t})]}{(k_2 - k_1)(k_3 - k_2)(k_3 - k_1)}$$

$$[\mathrm{G}] = [\mathrm{MLCT}]_0 - [\mathrm{MLCT}] - [^3\mathrm{MC}] - [^5\mathrm{MC}]$$

The long lifetime of the ^{5}MC excited state allows us to set $k_3 \cong 0$ when we model the kinetics in the first couple of picoseconds. The integrated rate equations can be reduced to,

$$[\mathrm{MLCT}] = [\mathrm{MLCT}]_0 e^{-k_1 t}$$

$$[^3\mathrm{MC}] = [\mathrm{MLCT}]_0 \frac{k_1}{k_2 - k_1}(e^{-k_1 t} - e^{-k_2 t})$$

$$[^5\mathrm{MC}] = [\mathrm{MLCT}]_0 (1 - \frac{k_2 e^{-k_1 t} - k_1 e^{-k_2 t}}{k_2 - k_1})$$

We repeated the analysis used for $[Fe(bpy)_3]^{2+}$ to analyze the $[Fe(bpy)_2(CN)_2]$ in methanol data. By combining the reference Kβ difference spectra with the two kinetic models, one with and one without the ^{3}MC intermediate, we fit the whole two dimensional time-dependent Kβ difference spectra. The fit parameters can be found in Table 1. The two dimensional time-dependent Kβ fluorescence spectrum, global fitting, residuals and the reconstructed population kinetics can be found in Figs. S2 and S3.

The residual sum of squares for each model is: RSS_1 = 2.52 and RSS_2 = 2.23. In this situation, we have p1 = 5, p2 = 6 and n = 45. To be 95% confident that complex model is better than the nested model, the calculated F value must be larger than the F distribution value that captures 95% of the distribution for F(p2-p1,n-p2) which is 4.09. The calculated F value is 5.08 which exceed 4.09. So with 95% confidence we conclude that the model containing the ^{3}MC intermediate provides a better description of the experimental data.

Fig. S2. [Fe(bpy)$_2$(CN)$_2$] in methanol two dimensional time-dependent Kβ fluorescence (A) experimental difference spectra and (B) fit using the sequential kinetic model with an intermediate. (C) Residuals for the best fit and (D) the excited state populations extracted from the best fit.

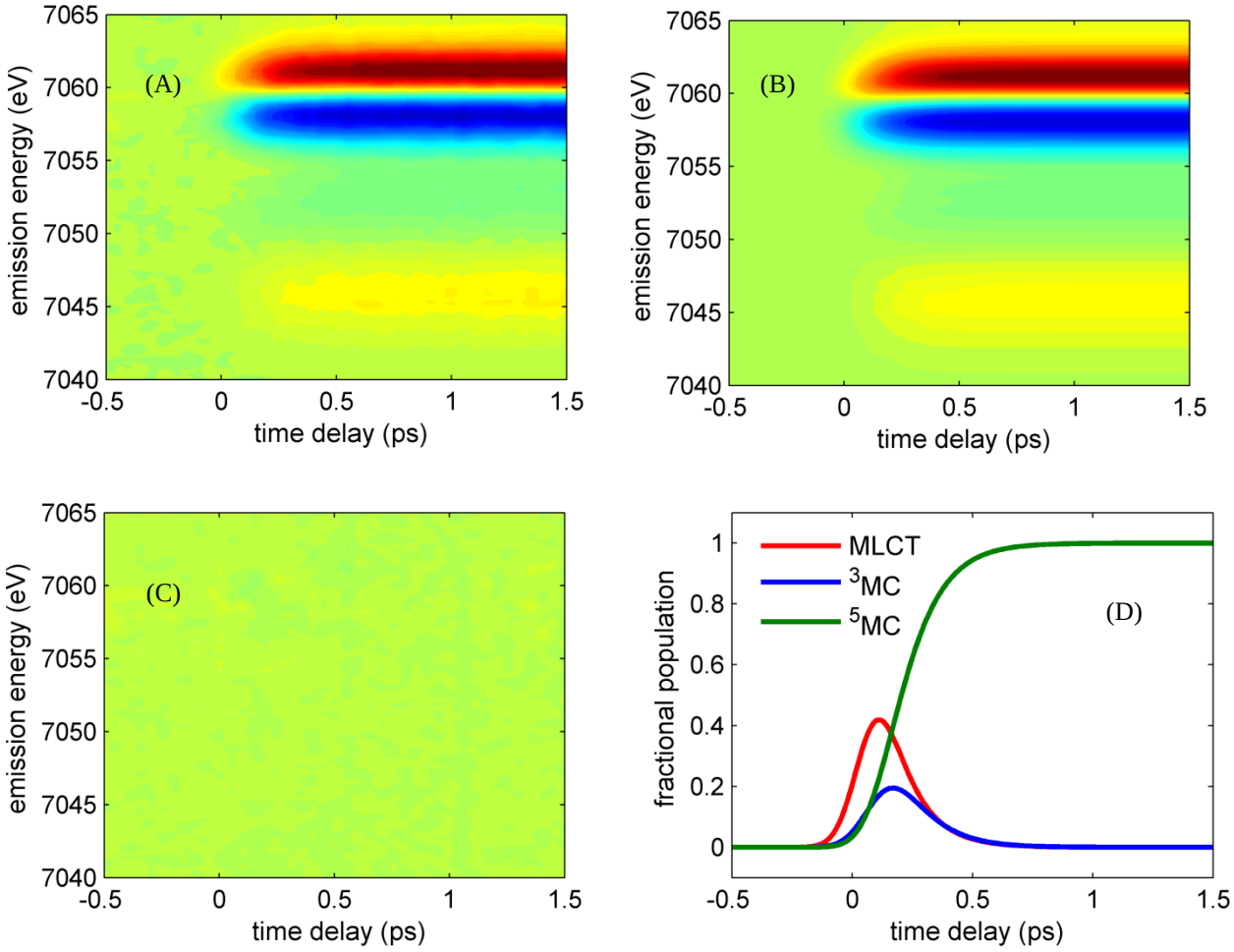

Fig. S3. $[Fe(2,2'\text{-bipyridine})_2(CN)_2]^0$ in methanol two dimensional time-dependent Kβ fluorescence (A) experimental difference spectra and (B) fit using the direct kinetic model without an intermediate. (C) Residuals for the best fit and (D) the excited state populations extracted from the best fit.

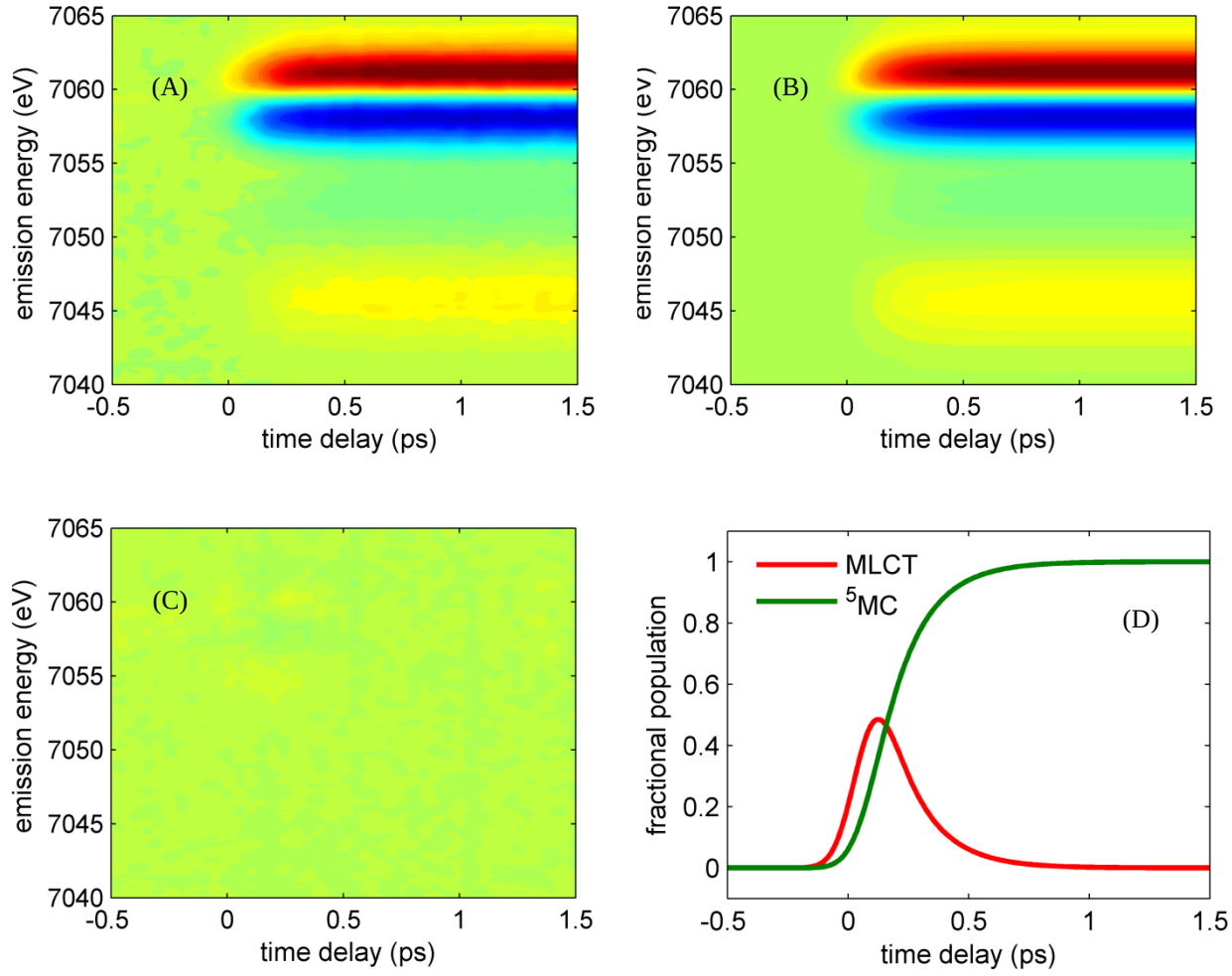

IV. References

[1] Y.Z. Liu, K.S. Kjaer, L.A. Fredin, P. Chabera, T. Harlang, S.E. Canton, S. Lidin, J.X. Zhang, R. Lomoth, K.E. Bergquist, P. Persson, K. Warnmark, V. Sundstrom, "A Heteroleptic Ferrous Complex with Mesoionic Bis(1,2,3-triazol-5-ylidene) Ligands: Taming the MLCT Excited State of Iron(II)," Chem.--Eur. J. 21 (9), 3628 (2015).

[2] W.K. Zhang, R. Alonso-Mori, U. Bergmann, C. Bressler, M. Chollet, A. Galler, W. Gawelda, R.G. Hadt, R.W. Hartsock, T. Kroll, K.S. Kjaer, K. Kubicek, H.T. Lemke, H.W. Liang, D.A. Meyer, M.M. Nielsen, C. Purser, J.S. Robinson, E.I. Solomon, Z. Sun, D. Sokaras, T.B. Van Driel, G. Vanko, T.C. Weng, D. Zhu, K.J. Gaffney, "Tracking Excited State Charge and Spin Dynamics in Iron Coordination Complexes " Nature 509 345 (2014).

[3] R. Alonso-Mori, J. Kern, D. Sokaras, T.C. Weng, D. Nordlund, R. Tran, P. Montanez, J. Delor, V.K. Yachandra, J. Yano, U. Bergmann, "A multi-crystal wavelength dispersive x-ray spectrometer," Rev. Sci. Instr. 83 (7), 9 (2012).

[4] L.J. Koerner, H.T. Philipp, M.S. Hromalik, M.W. Tate, S.M. Gruner, "X-ray tests of a Pixel Array Detector for coherent x-ray imaging at the Linac Coherent Light Source," J. Instrum. 4 8 (2009).

[5] R. Alonso-Mori, J. Kern, R.J. Gildea, D. Sokaras, T.C. Weng, B. Lassalle-Kaiser, R. Tran, J. Hattne, H. Laksmono, J. Hellmich, C. Glockner, N. Echols, R.G. Sierra, D.W. Schafer, J. Sellberg, C. Kenney, R. Herbst, J. Pines, P. Hart, S. Herrmann, R.W. Grosse-Kunstleve, M.J. Latimer, A.R. Fry, M.M. Messerschmidt, A. Miahnahri, M.M. Seibert, P.H. Zwart, W.E. White, P.D. Adams, M.J. Bogan, S. Boutet, G.J. Williams, A. Zouni, J. Messinger, P. Glatzel, N.K. Sauter, V.K. Yachandra, J. Yano, U. Bergmann, "Energy-dispersive X-ray emission spectroscopy using an X-ray free-electron laser in a shot-by-shot mode," Proc. Natl. Acad. Sci. U. S. A. 109 (47), 19103 (2012).

[6] M. Harmand, R. Coffee, M.R. Bionta, M. Chollet, D. French, D. Zhu, D.M. Fritz, H.T. Lemke, N. Medvedev, B. Ziaja, S. Toleikis, M. Cammarata, "Achieving few-femtosecond time-sorting at hard X-ray free-electron lasers," Nature Photon. 7 215 (2013).